Letter

Exciton- and light-induced ferromagnetism from doping a moiré Mott insulator

Hui Yang and Ya-Hui Zhang
Department of Physics and Astronomy, Johns Hopkins University, Baltimore, Maryland 21218, USA

Significant efforts have been dedicated to achieving excitonic insulators. In this paper, we explore a problem of doping excitons into a Mott insulator instead of a band insulator. Specifically, we start with a Mott insulator on a triangular moiré superlattice in a transition metal dichalcogenides layer and inject excitons by either transferring particles to a different layer or optically pumping electrons from the valence to the conduction band. In both cases, the excitons move in the presence of local spin moments inherited from the Mott insulator. When the Heisenberg spin coupling J is small, the kinetic energy of the excitons decides the magnetism, akin to Nagaoka ferromagnetism in hole-doped Mott insulators. Through density-matrix renormalization-group calculations, we demonstrate that the spin moments originating from the Mott insulator form $120°$ antiferromagnetic or ferromagnetic order for the two signs of the exciton hoppings over a broad range of exciton densities. Notably, the optical pump case may result in an antiferromagnetic to ferromagnetic transition with increasing exciton density, indicating a potential mechanism for light-induced ferromagnetism. A similar exciton-induced ferromagnetism could be achieved in a moiré-monolayer system where the monolayer is electron-doped while the moiré Mott insulator is hole-doped. Our works demonstrates a possibility to engineering magnetism through doping neutral excitons.

Introduction. Excitonic insulators have been the focus of much research attention over the past few decades [1–4]. Recent experimental advances in two-dimensional materials have opened up new avenues for investigating exciton physics [5–13]. In this article, we explore a direction where excitons are doped into a Mott insulator instead of a simple band insulator. Mott insulators have been known to host fascinating quantum phenomena such as frustrated magnetism and quantum spin liquids [14], owing to the presence of localized spin moments. Doping a Mott insulator with fermionic charge carriers has been a major focus of modern condensed-matter physics due to its connection to the high-temperature superconducting cuprates [15]. However, doping a Mott insulators with bosonic charge carriers has been comparatively underexplored, both theoretically and experimentally. Despite this, the interplay between the mobile carriers and the localized spin moments still suggests the possibility of intriguing quantum phases for bosonic carriers. In recent years, significant advancements in experimental techniques have enabled the injection of excitons into a moiré Mott insulator based on transition metal dichalcogenide (TMD) bilayers [16–23] As a result, it has become increasingly crucial to develop theoretical models and predictions for exciton-doped Mott insulators, which is precisely what we aim to accomplish in this paper.

Moiré superlattices are exceptional platforms for investigating strongly correlated physics [24–27]. Among these, moiré superlattices based on TMD hetero-bilayer and homo-bilayer have shown promising results in simulating Hubbard model physics [28–33]. A plethora of experimental discoveries have already been made, including Mott insulator [34,35], generalized Wigner crystal [35,36], continuous metal insulator transition [37,38], quantum anomalous Hall effect [39], and Kondo physics [40]. Building on the existing research, we now investigate the effects of doping neutral excitons into the Mott insulator. This can be achieved through two methods: transferring particles to a different layer using a displacement field in a bilayer system [16,17], or optically pumping electrons from the valence band to the conduction band [13,19,41–47]. We primarily focus on the former approach, as the equilibrium excitons in this case do not have a limited lifetime. However, it is important to note that our model and predictions also apply to optically pumped excitons within their lifetime. Many previous studies have used excitons to probe correlated states [48–51], but in this work, we focus on the novel physics that arises from a finite density of excitons.

Let us consider a bilayer system consisting of a moiré layer at the bottom and a monolayer TMD at the top, separated by an insulating hBN barrier. Initially, the system has $n_b = 1$ and $n_t = 0$, where $n_{b(t)}$ is the number of particles per site in the bottom (top) layer, resulting in the moiré layer being in a Mott insulating phase. Our first step is to obtain Wannier orbitals of the exciton by solving Schrödinger's equations with one single vacancy or two nearby vacancies in the moiré layer. This approach leads to an effective low-energy spin-exciton model with four states on each moiré site: (1) one hole in the moiré layer with spin up;[1] (2) one hole in the moiré layer with spin down; (3) one exciton with spin up in the monolayer; and (4) one exciton with spin down in the monolayer. It is important to note that a hole and an exciton cannot simultaneously occupy the same site. Our model in Eq. (2) involves four crucial parameters: the hopping of the excitons (J_p), the repulsive interaction between two nearby excitons (J_{pz}), the

---

[1]The particle can be an electron or hole depending whether we dope into the conduction or valence band.

spin-spin coupling in the monolayer (J_t), and the spin-spin coupling in the moiré layer (J_b). Specifically, we are interested in the regime with $n_b = 1 - x$ and $n_t = x$, where x denotes the exciton density. Our model is particularly suited for the small-x regime, where the excitons remain stable against dissociation into an electron-hole gas.

We then employ density-matrix renormalization-group [52] (DMRG) technique to simulate the model. Our focus is on the regime where J_b is small or zero, which is a reasonable assumption for a strong Mott insulator with a large U/t, as demonstrated in the TMD hetero-bilayer [34]. In this regime, the magnetism of the localized spin moments in the moiré Mott layer is primarily governed by the kinetic energy of the excitons, akin to the Nagaoka ferromagnetism [53] and kinetic antiferromagnetism [54–57] in the hole-doped Mott insulator, which is different from the magnetic order controlled by spin-orbit coupling studied in Ref. [58]. Specifically, we observe a 120° antiferromagnetic order or a ferromagnetic order for $J_p > 0$ and $J_p < 0$, respectively, where the sign of exciton hopping (J_p) plays a pivotal role. The latter is realized if we hole-dope the moiré layer with $n_b^h = 1 + x$ holes in the valence band while electron-doping the monolayer with $n_t^e = x$ electrons in the conduction band. In this case there is an antiferromagnetic-to-ferromagnetic transition when increasing the exciton density x if there is a finite but small J_b at $x = 0$. The same conclusion holds true in the case of optically pumped excitons, offering a plausible mechanism for light-induced ferromagnetism. This picture may also be relevant to the experimental findings in Ref. [19].

Model. We consider the experimental setup shown in Fig. 1(a). We have a moiré superlattice formed by a WSe$_2$/WS$_2$ hetero-bilayer in the bottom, separated from a WSe$_2$ monolayer in the top by an insulating hexagon boron nitride (hBN) barrier. We call this setup moiré + monolayer. Because interlayer tunneling is suppressed by the hBN barrier, which is different from the two-orbital Hubbard model [59–63], the top and bottom WSe$_2$ layer have separately conserved total number of charges. Both the moiré layer in the bottom and the monolayer in the top can be either electron or hole doped from the charge neutrality, which is a band insulator with large band gap on order of 1 eV. To avoid confusion, we define electron (or hole) density per moiré unit cell of the layer $a = t, b$ as n_a^e (or n_a^h). The total charge density at layer a is thus $\rho_a = n_a^h - n_a^e$. Our starting point is $n_b^h = 1$, $n_t = 0$, where the bottom moiré layer forms a Mott insulator with one hole per moiré site while the top layer is still at charge neutrality. Then we dope excitons in two different ways: (I) We tune the density to be $n_b^h = 1 - x$, $n_t = x$, shown in Fig. 1(b). (II) We tune the density to be $n_b^h = 1 + x$, $n_t^e = x$, shown in Fig. 1(c). In the first case, we have excitons formed by a vacancy of hole in the valence band of the bottom layer and a hole in the valence band of the top layer. In the second case, we have excitons formed by an additional hole in the valence band of the bottom layer and an electron in the conduction band of the top layer. We see later that these two cases can be captured by similar effective model, but with opposite signs of the hopping of excitons, which will qualitatively change the magnetic physics of the localized spin moments in the bottom moiré layer. Both these cases can be achieved in equilibrium with a displacement field D in a dual gated sample to tune the
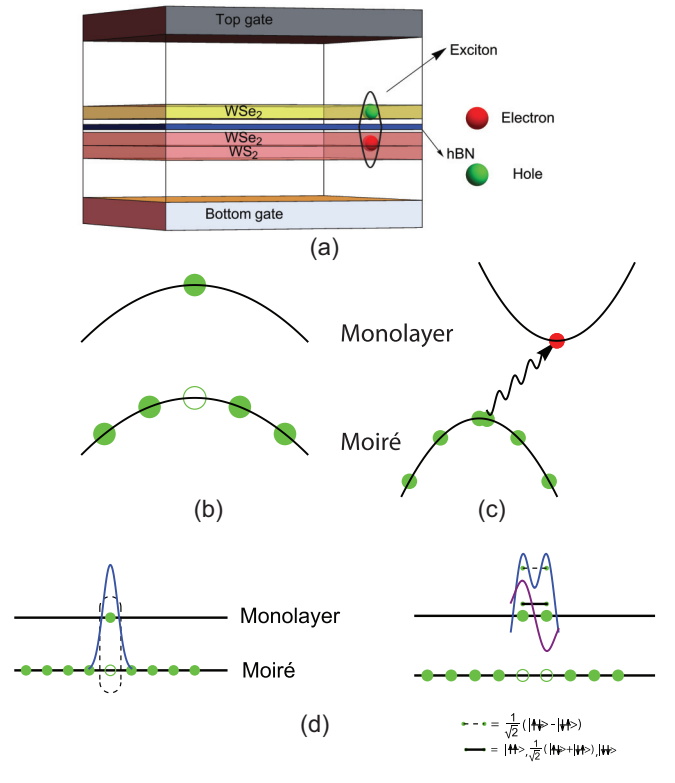

FIG. 1. (a) An illustration of the moiré (WS$_2$/WSe$_2$) + monolayer (WSe$_2$) system. (b), (c) Two different ways of doping excitons into a Mott insulator. Here, the solid red circle denotes an electron in the conduction band, and empty red labels a vacancy of electron in the conduction band. Similarly, a solid green circle means a hole in the valence band, while an empty green circle means a vacancy of a hole in the valence band. A vacancy of a hole is equivalent to an electron in the valence band, but we call it vacancy of a hole to distinguish it from an electron in the conduction band. (b) $n_b^h = 1 - x$, $n_t^h = x$. (c) $n_b^h = 1 + x$, $n_t^e = x$. (d) Illustration of the wave function of the holes in the top layer when there is one vacancy (on the left), and two vacancies (on the right) doped into the moiré Mott insulator in the bottom. When there are two vacancies nearby, the two holes form a spin singlet or a spin triplet, whose energy difference gives the parameter J_t in our model in Eq. (2).

densities of the top and bottom layers separately. The second case can also be realized in nonequilibrium through optical pumping.

We focus on the case I as an example to derive a low-energy effective model to capture the exciton and magnetic moments. We start from the Mott insulator in the moiré layer, which is captured by an extended lattice Hubbard model [28–33]:

$$H_b = -t_b \sum_{\langle ij \rangle} h_{bi\sigma}^\dagger h_{bj\sigma} + \frac{U}{2} \sum_i n_{bi}^2 + V \sum_{\langle ij \rangle} n_{bi} n_{bj}, \quad (1)$$

where $h_{bj\sigma}^\dagger$ ($h_{bj\sigma}$) is the creation (annihilation) operator for spin σ, and $n_{bi} = \sum_\sigma h_{bj\sigma}^\dagger h_{bj\sigma}$ is the particle number operator. From our calculation (see Supplemental Material [64]), we get $t_b = 1.06$ meV, $U = 660.635/\epsilon$ meV, and $V = 92.689/\epsilon$ meV, where ϵ is the renormalization factor of the dielectric constant, which should be on the order of ten.
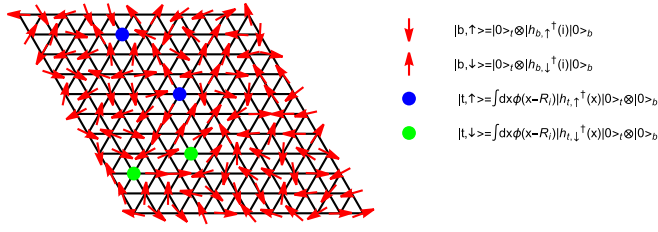
FIG. 2. Illustration of the moiré lattice and the four-dimensional local Hilbert space. The local moments represent the spin degree of freedom in the bottom layer. The solid disks represent the doped excitons with density x. Different colors correspond to different spins in the top layer of the exciton state. If we polarize the spin in the top layer, there is one flavor for exciton and the model reduces to a bosonic version of t-J model.

FIG. 3. The couplings in our effective model as a function of the dielectric constant ϵ. The vertical axis on the left is for J_{pz} and J_t, and the vertical axis on the right is for J_p. In our calculation, the lattice constants are 0.328 nm for WSe$_2$, 0.315 nm for WS$_2$, and the moiré lattice constant is $a_M = 7.9$ nm at zero twist angle. $m = 0.42m_e$ is the effective mass for the valence band of WSe$_2$. The distance of the top layer and bottom layer is $d = 2nm$ (see Supplemental Material [64]).

The Mott insulator has one hole per moiré site in the bottom layer. When the system is doped with one hole in the top layer and one vacancy of hole (electron) in the bottom layer, the hole in the top layer will be trapped to the vacancy of hole in the bottom layer, leading to a neutral exciton. Let us treat the t_b term as a small perturbation and ignore it for now. Then the vacancy in the bottom layer is fixed at one site i. The hole in the top layer moves under the potential $\sum_{j\neq i} V_j(x)$, where $V_j(x)$ is the Coulomb interaction between the hole in the top layer and the hole at moiré site j of the bottom layer. We can get the wave function $\psi_i(x - \mathbf{R}_i)$ for the hole in the top layer by solving the corresponding Schrödinger equation. As schematically shown in Fig. 1(d), the hole wave function is very localized around the vacancy site $\mathbf{R}_i$. Combining the two spins of the hole in the top layer, we have two exciton states [65] $|t, \sigma\rangle = \int dx \psi_i(x - R_i) h_{t\sigma}^\dagger(x) |0\rangle_t |0\rangle_b$ for each site i. We have two additional states without exciton at site i: $|b, \sigma\rangle = h_{i;b\sigma}^\dagger |0\rangle_b \otimes |0\rangle_t$. Here $\sigma = \uparrow, \downarrow$. These four states are shown in Fig. 2. Because of the strong interlayer repulsion, doubly occupied states with holes in both top and bottom layer at the same site are penalized and ignored.

Now we can proceed to derive the effective hopping of the exciton. The four states at each site can be constructed from a tensor product of a layer pseudospin $1/2$ $\vec{P}$ and the real spin $\vec{S}$ [22]. Then the exciton creation and annihilation operator correspond to $P^\dagger$ and P^-. The spin operator in the top layer is $\vec{S}_t(i) = \frac{1}{2}(1 + P_z)\vec{S}(i)$, while the spin operator in the bottom layer is $\vec{S}_b(i) = \frac{1}{2}(1 - P_z)\vec{S}(i)$. $\vec{P}_z(i)$ is the layer polarization or equivalently a dipole moment. $1 + P_z(i)$ is the exciton occupation number at the site i. With these operators, an effective four-flavor model can be written down:

$$H = \sum_{\langle ij \rangle} J_t \vec{S}_t(i) \cdot \vec{S}_t(j) + J_b \vec{S}_b(i) \cdot \vec{S}_b(j) + \frac{1}{2} J_{pz} P_z(i) P_z(j)$$

$$+ \frac{1}{2} J_p [P_x(i) P_x(j) + P_y(i) P_y(j)](4\vec{S}(i) \cdot \vec{S}(j) + S_0(i) S_0(j)), \quad (2)$$

where J_p is the exciton hopping. The exciton hopping corresponds to hole in the top layer and electron in the bottom layer hopping simultaneously. From the first-order perturbation of the t_b term, we get $J_p = t_b \int \psi_i^*(x - R_i)\psi_j(x - R_j)$ as the exciton hopping. $J_{pz}/8$ gives the dipole-dipole repulsion
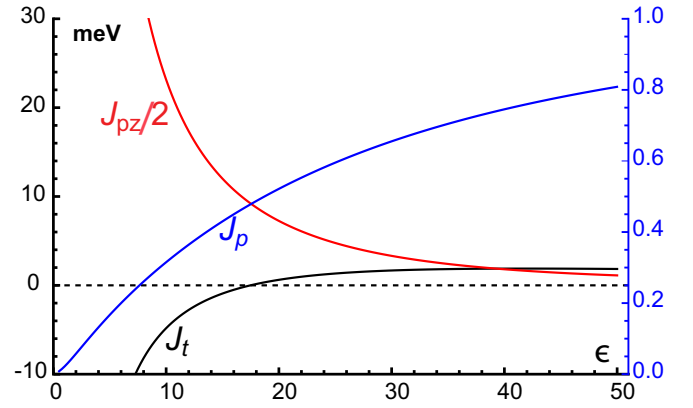
for two nearby excitons. J_b is the superexchange spin coupling of the bottom layer, which we assume is small in the strong-U_b/t_b limit. J_t is the spin-spin coupling in the top layer, which has two competing contributions: Hund's coupling to favor spin-triplet and covalent bonding to favor spin-singlet. The evolution of these parameters with the dielectric constant ϵ is shown in Fig. 3. When $\epsilon = 20$, we have $J_{pz}/2 = 7.25075$ meV, $J_p = 0.51646$ meV, $J_t = 0.621032$ meV, here $J_p = 0.487t_b$ here we use $t_b = 1.06$ meV as derived from Wannier orbital construction. $J_b = 4t_b^2/U \approx 0.14$ meV and is smaller than other values. In our derivation, the physics of exciton is from the first perturbation, however, the spin polaron is controlled by J_b, which is second order of t_b. Thus in this paper, we focus on the effects of excitons.

So far we have discussed case I. In case II, we dope an additional hole in the bottom layer, accompanied by an electron in the conduction band of the top layer. The physics is described by the same model as in case I, except now the hopping term J_p is negative. The effective hopping of an exciton is from a second-order process of hopping electron and hole. In the case I electron and hole are from the same valence band, while in the case II they are from conduction and valence band. This gives a sign difference.

Reduction to a bosonic t-J model. Let us assume that the spin of the top layer is polarized spin up. Then the four states at each site reduces to three states; we can label them $|\uparrow\rangle = |b, \uparrow\rangle, |\downarrow\rangle = |b, \downarrow\rangle, |0\rangle = |t, \uparrow\rangle$. One can see that the Hilbert space is similar to the familiar t-J model with the exciton state playing the role of the empty site. The difference is that the doped carriers are neutral and bosonic. Nevertheless, we expect the influence to the magnetism may be similar to the fermionic t-J model, especially when x is small. We confirm this picture below.

Exciton-induced magnetism. When the exciton density x is zero, the magnetic physics in the bottom layer is governed by the superexchange Heisenberg coupling $J_b \approx 4t_b^2/U$. We
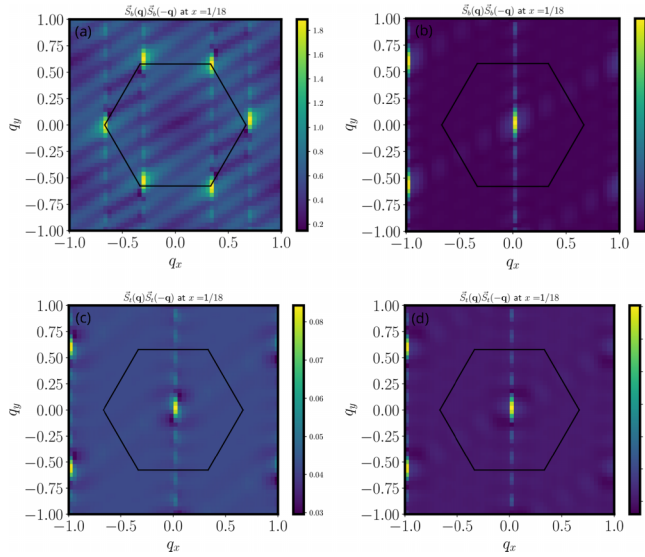
FIG. 4. The spin-spin correlation function for fixed $J_b = J_t = 0$, $J_{pz} = 5$, $x = 1/18$. Panels (a) and (b) show the spin-correlation function $\langle \vec{S}_b(\mathbf{q}) \vec{S}_b(-\mathbf{q}) \rangle$ in the bottom layer, and panels (c) and (d) show the spin-correlation function $\langle \vec{S}_t(\mathbf{q}) \vec{S}_t(-\mathbf{q}) \rangle$ in the top layer. Panels (a) and (c) show the results for $J_p = 1$. Panels (b) and (d) show the results for $J_p = -1$.

focus on the regime where $U \gg t_b$ and J_b is very small, as observed in the TMD hetero-bilayer at zero twist angle. Then at $x = 0$ all of the spin configurations are degenerate. Here we are interested in how the movement of excitons influence the magnetic ordering at finite x.

We see that the spin $\vec{S}_t$ in the top layer is spin polarized. Then as said before the physics is captured by a bosonic version of the t-J model. If there is only one single exciton, then the statistics does not matter and it is equivalent to the familiar fermionic t-J model with a single hole. So we can quote the previous studies of the fermionic t-J model to understand our system. In the single hole doped Mott insulator, it is known that the magnetic ordering in the infinite U limit is decided by the kinetic energy of the holes, which leads to either the 120° antiferromagnetic (AFM) order [54–57] or the Nagaoka ferromagnetic order (FM) depending on the sign of the hopping [53]. Following this mapping, we reach the conclusion

that the magnetic order of $\vec{S}_b$ is 120° AFM if $J_p > 0$ and spin polarized if $J_p < 0$ for the single exciton case.

To check whether the conclusion holds for finite densities of excitons, we adopt infinite density-matrix renormalization-group [66] (iDMRG) to simulate the model Eq. (2). The iDMRG simulation is performed on $L_x \times L_y = 6 \times 6$ cylinder. L_x is along the direction $\mathbf{a}_1 = (1, 0)$ and L_y is along the direction $\mathbf{a}_2 = (-1/2, \sqrt{3}/2)$. The bond dimension is up to 5000 and the truncation error is 10^{-5}. The exciton density x is from $1/18$ to $17/18$.

We first fix $J_b = J_t = 0$ and $J_{pz} = 5$, so the spin configurations are selected purely by the exciton hopping term J_p. The spin structure factors are shown in Fig. 4. At $x = 1/18$, for $J_p = 1$, in Figs. 4(a) and 4(c). We can read that the spin in the bottom moiré layer is 120° ordered, while the spin in the top layer is ferromagnetically ordered. In contrast, if $J_p = -1$, as shown in Figs. 4(b) and 4(d), the spin in both layers are now FM ordered. The spin configuration in the bottom moiré layer exactly follows our expectation from analog to the hole-doped case. There is an intuitive explanation in Schwinger boson mean-field theory which we list in the Supplemental Material [64]. Once the magnetic order in the bottom layer is fixed, the exciton only carries the spin $1/2$ in the top layer and we have spinful boson gas with density x, which is known to be in a spin-polarized Bose-Einstein condensation (BEC) phase. This explains the FM order of the top layer. The case of $J_p < 0$ is particularly interesting because the FM order is quite robust against large exciton density (see Supplemental Material [64]). $J_p < 0$ can be realized in the case II, with electron and hole doped into the conduction and valence band of the two layers, respectively. In real systems there may be a small but finite $J_b > 0$. Then there is a competition between the AFM order from J_b and the kinetic FM. In Fig. 5, we show a transition from an antiferromagnetic state to a ferromagnetic state in the bottom layer as we increase the exciton density, while the spin in the top layer is always polarized during this transition [64]. In the FM phase we also have exciton condensed at momentum $Q = 0$, forming a spin-polarized superfluid [64]. Note that case II can also be realized with optical pumping, with exciton density proportional to the optical power. Hence this provides a mechanism of light-induced ferromagnetism. Light-induced FM was observation recently [19] at fractional total filling, $n = -1/3$. Similar model can be
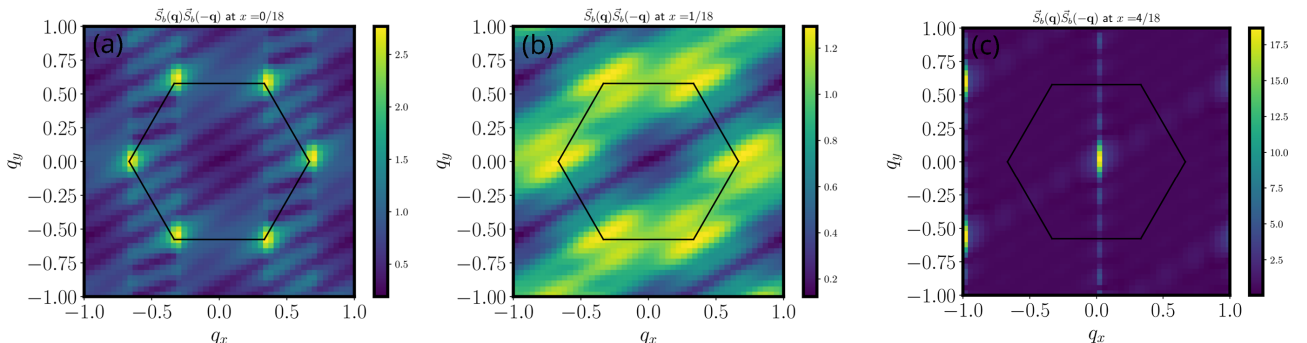

FIG. 5. (a), (b) The spin-correlation function $\langle \vec{S}_b(\mathbf{q}) \vec{S}_b(-\mathbf{q}) \rangle$ for fixed $J_t = 0$, $J_{pz} = 5$, $J_p = -1$, $J_b = 0.06$. Panels (a)–(c) correspond to the increasing of exciton density.

shown to describe exciton doped Wigner crystal at $n = -1/3$ [64] and thus our theory may offer a natural explanation of the observation in Ref. [19] in terms of kinetic-driven ferromagnetism.

Conclusion. In summary, we study exciton-doped Mott insulator in the TMD moiré systems. In these systems the spin-spin coupling J of the Mott insulator is usually very small because U/t is very large. As a result, the magnetism of the localized moments will be decided by the kinetic term of the exciton. We perform a DMRG simulation and find that the spin moments inherited from the Mott insulator form $120°$ AFM order or ferromagnetic order depending on the sign of the effective hopping of excitons. Especially, if we dope a moiré+monolayer with electron and hole in the two layers, respectively, there

can be an antiferromagnetic-to-ferromagnetic transition when increasing the exciton density. The same physics can happen through optical pumping, providing a mechanism of light-induced ferromagnetism. Our work demonstrates the possibility of engineering magnetism through doping neutral excitons.

[1] D. Jérome, T. M. Rice, and W. Kohn, Phys. Rev. **158**, 462 (1967).

[2] J. Zittartz, Phys. Rev. **164**, 575 (1967).

[3] B. I. Halperin and T. M. Rice, J. Phys. C: Solid State Phys. **21**, 115 (1968).

[4] C. Comte and P. Nozières, J. Phys. (Paris) **43**, 1069 (1982).

[5] J. Eisenstein, Annu. Rev. Condens. Matter Phys. **5**, 159 (2014).

[6] J. I. A. Li, T. Taniguchi, K. Watanabe, J. Hone, and C. R. Dean, Nat. Phys. **13**, 751 (2017).

[7] X. Liu, K. Watanabe, T. Taniguchi, B. I. Halperin, and P. Kim, Nat. Phys. **13**, 746 (2017).

[8] G. Wang, A. Chernikov, M. M. Glazov, T. F. Heinz, X. Marie, T. Amand, and B. Urbaszek, Rev. Mod. Phys. **90**, 021001 (2018).

[9] A. Kogar, M. S. Rak, S. Vig, A. A. Husain, F. Flicker, Y. I. Joe, L. Venema, G. J. MacDougall, T. C. Chiang, E. Fradkin, J. van Wezel, and P. Abbamonte, Science **358**, 1314 (2017).

[10] Z. Wang, D. A. Rhodes, K. Watanabe, T. Taniguchi, J. C. Hone, J. Shan, and K. F. Mak, Nature (London) **574**, 76 (2019).

[11] N. P. Wilson, W. Yao, J. Shan, and X. Xu, Nature (London) **599**, 383 (2021).

[12] Y. Jia, P. Wang, C.-L. Chiu, Z. Song, G. Yu, B. Jäck, S. Lei, S. Klemenz, F. A. Cevallos, M. Onyszczak, N. Fishchenko, X. Liu, G. Farahi, F. Xie, Y. Xu, K. Watanabe, T. Taniguchi, B. A. Bernevig, R. J. Cava, L. M. Schoop *et al.*, Nat. Phys. **18**, 87 (2022).

[13] E. C. Regan, D. Wang, E. Y. Paik, Y. Zeng, L. Zhang, J. Zhu, A. H. MacDonald, H. Deng, and F. Wang, Nat. Rev. Mater. **7**, 778 (2022).

[14] L. Balents, Nature (London) **464**, 199 (2010).

[15] P. A. Lee, N. Nagaosa, and X.-G. Wen, Rev. Mod. Phys. **78**, 17 (2006).

[16] J. Gu, L. Ma, S. Liu, K. Watanabe, T. Taniguchi, J. C. Hone, J. Shan, and K. F. Mak, Nat. Phys. **18**, 395 (2022).

[17] Z. Zhang, E. C. Regan, D. Wang, W. Zhao, S. Wang, M. Sayyad, K. Yumigeta, K. Watanabe, T. Taniguchi, S. Tongay, M. Crommie, A. Zettl, M. P. Zaletel, and F. Wang, Nat. Phys. **18**, 1214 (2022).

[18] Y. Xu, K. Kang, K. Watanabe, T. Taniguchi, K. F. Mak, and J. Shan, Nat. Nanotechnol. **17**, 934 (2022).

[19] X. Wang, C. Xiao, H. Park, J. Zhu, C. Wang, T. Taniguchi, K. Watanabe, J. Yan, D. Xiao, D. R. Gamelin, W. Yao, and X. Xu, Nature (London) **604**, 468 (2022).

[20] D. Chen, Z. Lian, X. Huang, Y. Su, M. Rashetnia, L. Ma, L. Yan, M. Blei, L. Xiang, T. Taniguchi, K. Watanabe, S. Tongay, D. Smirnov, Z. Wang, C. Zhang, Y.-T. Cui, and S.-F. Shi, Nat. Phys. **18**, 1171 (2022).

[21] Y.-H. Zhang, D. N. Sheng, and A. Vishwanath, Phys. Rev. Lett. **127**, 247701 (2021).

[22] Y.-H. Zhang, Phys. Rev. B **106**, 195120 (2022).

[23] T.-S. Huang, Y.-Z. Chou, C. L. Baldwin, F. Wu, and M. Hafezi, Phys. Rev. B **107**, 195151 (2023).

[24] Y. Cao, V. Fatemi, A. Demir, S. Fang, S. L. Tomarken, J. Y. Luo, J. D. Sanchez-Yamagishi, K. Watanabe, T. Taniguchi, E. Kaxiras, R. C. Ashoori, and P. Jarillo-Herrero, Nature (London) **556**, 80 (2018).

[25] Y. Cao, V. Fatemi, S. Fang, K. Watanabe, T. Taniguchi, E. Kaxiras, and P. Jarillo-Herrero, Nature (London) **556**, 43 (2018).

[26] E. Andrei, D. Efetov, P. Jarillo-Herrero, A. MacDonald, K. Mak, T. Senthil, E. Tutuc, A. Yazdani, and A. Young, Nat. Rev. Mater. **6**, 201 (2021).

[27] K. F. Mak and J. Shan, Nat. Nanotechnol. **17**, 686 (2022).

[28] F. Wu, T. Lovorn, E. Tutuc, and A. H. MacDonald, Phys. Rev. Lett. **121**, 026402 (2018).

[29] F. Wu, T. Lovorn, E. Tutuc, I. Martin, and A. H. MacDonald, Phys. Rev. Lett. **122**, 086402 (2019).

[30] Y. Zhang, N. F. Q. Yuan, and L. Fu, Phys. Rev. B **102**, 201115(R) (2020).

[31] H. Pan, F. Wu, and S. Das Sarma, Phys. Rev. B **102**, 201104(R) (2020).

[32] H. Pan and S. Das Sarma, Phys. Rev. Lett. **127**, 096802 (2021).

[33] J. Zang, J. Wang, J. Cano, A. Georges, and A. J. Millis, Phys. Rev. X **12**, 021064 (2022).

[34] Y. Tang, L. Li, T. Li, Y. Xu, S. Liu, K. Barmak, K. Watanabe, T. Taniguchi, A. H. MacDonald, J. Shan, and K. F. Mak, Nature (London) **579**, 353 (2020).

[35] E. C. Regan, D. Wang, C. Jin, M. I. Bakti Utama, B. Gao, X. Wei, S. Zhao, W. Zhao, Z. Zhang, K. Yumigeta, M. Blei, J. D. Carlström, K. Watanabe, T. Taniguchi, S. Tongay, M. Crommie, A. Zettl, and F. Wang, Nature (London) **579**, 359 (2020).

[36] H. Li, S. Li, E. C. Regan, D. Wang, W. Zhao, S. Kahn, K. Yumigeta, M. Blei, T. Taniguchi, K. Watanabe *et al.*, arXiv:2106.10599.

[37] T. Li, S. Jiang, L. Li, Y. Zhang, K. Kang, J. Zhu, K. Watanabe, T. Taniguchi, D. Chowdhury, L. Fu, J. Shan, and K. F. Mak, Nature (London) **597**, 350 (2021).

[38] A. Ghiotto, E.-M. Shih, G. S. S. G. Pereira, D. A. Rhodes, B. Kim, J. Zang, A. J. Millis, K. Watanabe, T. Taniguchi, J. C. Hone, L. Wang, C. R. Dean, and A. N. Pasupathy, Nature (London) **597**, 345 (2021).

[39] T. Li, S. Jiang, B. Shen, Y. Zhang, L. Li, Z. Tao, T. Devakul, K. Watanabe, T. Taniguchi, L. Fu, J. Shan, and K. F. Mak, Nature (London) **600**, 641 (2021).

[40] W. Zhao, B. Shen, Z. Tao, Z. Han, K. Kang, K. Watanabe, T. Taniguchi, K. F. Mak, and J. Shan, Nature (London) **616**, 61 (2023).

[41] C. Jin, E. C. Regan, A. Yan, M. I. B. Utama, D. Wang, S. Zhao, Y. Qin, S. Yang, Z. Zheng, S. Shi, K. Watanabe, T. Taniguchi, S. Tongay, A. Zettl, and F. Wang, Nature (London) **567**, 76 (2019).

[42] R. Xiong, J. H. Nie, S. L. Brantly, P. Hays, R. Sailus, K. Watanabe, T. Taniguchi, S. Tongay, and C. Jin, Science **380**, 860 (2023).

[43] K. L. Seyler, P. Rivera, H. Yu, N. P. Wilson, E. L. Ray, D. G. Mandrus, J. Yan, W. Yao, and X. Xu, Nature (London) **567**, 66 (2019).

[44] K. Tran, G. Moody, F. Wu, X. Lu, J. Choi, K. Kim, A. Rai, D. A. Sanchez, J. Quan, A. Singh, J. Embley, A. Zepeda, M. Campbell, T. Autry, T. Taniguchi, K. Watanabe, N. Lu, S. K. Banerjee, K. L. Silverman, S. Kim *et al.*, Nature (London) **567**, 71 (2019).

[45] E. M. Alexeev, D. A. Ruiz-Tijerina, M. Danovich, M. J. Hamer, D. J. Terry, P. K. Nayak, S. Ahn, S. Pak, J. Lee, J. I. Sohn, M. R. Molas, M. Koperski, K. Watanabe, T. Taniguchi, K. S. Novoselov, R. V. Gorbachev, H. S. Shin, V. I. Fal'ko, and A. I. Tartakovskii, Nature (London) **567**, 81 (2019).

[46] L. Zhang, F. Wu, S. Hou, Z. Zhang, Y.-H. Chou, K. Watanabe, T. Taniguchi, S. R. Forrest, and H. Deng, Nature (London) **591**, 61 (2021).

[47] B. Gao, D. G. Suárez-Forero, S. Sarkar, T.-S. Huang, D. Session, M. J. Mehrabad, R. Ni, M. Xie, P. Upadhyay, J. Vannucci, S. Mittal, K. Watanabe, T. Taniguchi, A. Imamoglu, Y. Zhou, and M. Hafezi, Nat. Commun. **15**, 2305 (2024).

[48] S. Miao, T. Wang, X. Huang, D. Chen, Z. Lian, C. Wang, M. Blei, T. Taniguchi, K. Watanabe, S. Tongay, Z. Wang, D. Xiao, Y.-T. Cui, and S.-F. Shi, Nat. Commun. **12**, 3608 (2021).

[49] E. Liu, T. Taniguchi, K. Watanabe, N. M. Gabor, Y.-T. Cui, and C. H. Lui, Phys. Rev. Lett. **127**, 037402 (2021).

[50] Y. Shimazaki, I. Schwartz, K. Watanabe, T. Taniguchi, M. Kroner, and A. Imamoğlu, Nature (London) **580**, 472 (2020).

[51] Y. Zhou, J. Sung, E. Brutschea, I. Esterlis, Y. Wang, G. Scuri, R. J. Gelly, H. Heo, T. Taniguchi, K. Watanabe, G. Zaránd, M. D. Lukin, P. Kim, E. Demler, and H. Park, Nature (London) **595**, 48 (2021).

[52] S. R. White, Phys. Rev. Lett. **69**, 2863 (1992).

[53] Y. Nagaoka, Phys. Rev. **147**, 392 (1966).

[54] J. O. Haerter and B. S. Shastry, Phys. Rev. Lett. **95**, 087202 (2005).

[55] M. Davydova, Y. Zhang, and L. Fu, Phys. Rev. B **107**, 224420 (2023).

[56] I. Morera, M. Kanász-Nagy, T. Smolenski, L. Ciorciaro, A. Imamoğlu, and E. Demler, Phys. Rev. Res. **5**, L022048 (2023).

[57] K. Lee, P. Sharma, O. Vafek, and H. J. Changlani, Phys. Rev. B **107**, 235105 (2023).

[58] J. Carlström, Phys. Rev. Res. **4**, 043126 (2022).

[59] K. Wohlfeld, S. Nishimoto, M. W. Haverkort, and J. van den Brink, Phys. Rev. B **88**, 195138 (2013).

[60] K. Wohlfeld, M. Daghofer, A. M. Oleś, and P. Horsch, Phys. Rev. B **78**, 214423 (2008).

[61] C.-C. Chen, M. van Veenendaal, T. P. Devereaux, and K. Wohlfeld, Phys. Rev. B **91**, 165102 (2015).

[62] K. Wohlfeld, M. Daghofer, S. Nishimoto, G. Khaliullin, and J. van den Brink, Phys. Rev. Lett. **107**, 147201 (2011).

[63] J. Schlappa, K. Wohlfeld, K. J. Zhou, M. Mourigal, M. W. Haverkort, V. N. Strocov, L. Hozoi, C. Monney, S. Nishimoto, S. Singh, A. Revcolevschi, J.-S. Caux, L. Patthey, H. M. Rønnow, J. van den Brink, and T. Schmitt, Nature (London) **485**, 82 (2012).

[64] See Supplemental Material at http://link.aps.org/supplemental/10.1103/PhysRevB.110.L041115 for the derivation of the effective model from the construction of the Wannier function, the derivation of the exciton bound state. We also give the details of the DMRG simulation, and we also give more detailed DMRG results, which also contains Refs. [19,22,68,69].

[65] C. Yang and A. E. Feiguin, Phys. Rev. B **98**, 035128 (2018).

[66] I. P. McCulloch, arXiv:0804.2509.

[67] J. Hauschild and F. Pollmann, SciPost Phys. Lect. Notes, 5 (2018), code available from https://github.com/tenpy/tenpy.

[68] Y.-H. Zhang and T. Senthil, Phys. Rev. B **99**, 205150 (2019).

[69] N. Marzari, A. A. Mostofi, J. R. Yates, I. Souza, and D. Vanderbilt, Rev. Mod. Phys. **84**, 1419 (2012).